



HAL
open science

Stark broadening measurements in plasmas produced by laser ablation of hydrogen containing compounds

Miloš Burger, Jorg Hermann

► **To cite this version:**

Miloš Burger, Jorg Hermann. Stark broadening measurements in plasmas produced by laser ablation of hydrogen containing compounds. *Spectrochimica Acta Part B: Atomic Spectroscopy*, 2016, 122, pp.118-126. 10.1016/j.sab.2016.06.005 . hal-02348424

HAL Id: hal-02348424

<https://hal.science/hal-02348424>

Submitted on 5 Nov 2019

HAL is a multi-disciplinary open access archive for the deposit and dissemination of scientific research documents, whether they are published or not. The documents may come from teaching and research institutions in France or abroad, or from public or private research centers.

L'archive ouverte pluridisciplinaire **HAL**, est destinée au dépôt et à la diffusion de documents scientifiques de niveau recherche, publiés ou non, émanant des établissements d'enseignement et de recherche français ou étrangers, des laboratoires publics ou privés.

Stark broadening measurements in plasmas produced by laser ablation of hydrogen containing compounds

Miloš Burger^{a,*}, Jörg Hermann^b

^aUniversity of Belgrade, Faculty of Physics, POB 44, 11000 Belgrade, Serbia

^bLP3, CNRS - Aix-Marseille University, 13008 Marseille, France

Abstract

We present a method for the measurement of Stark broadening parameters of atomic and ionic spectral lines based on laser ablation of hydrogen containing compounds. Therefore, plume emission spectra, recorded with an echelle spectrometer coupled to a gated detector, were compared to the spectral radiance of a plasma in local thermal equilibrium. Producing material ablation with ultraviolet nanosecond laser pulses in argon at near atmospheric pressure, the recordings take advantage of the spatially uniform distributions of electron density and temperature within the ablated vapor. By changing the delay between laser pulse and detector gate, the electron density could be varied by more than two orders of magnitude while the temperature was altered in the range from 6,000 to 14,000 K. The Stark broadening parameters of transitions were derived from their simultaneous observation with the hydrogen Balmer alpha line. In addition, assuming a linear increase of Stark widths and shifts with electron density for non-hydrogenic lines, our measurements indicate a change of the Stark broadening-dependence of H_α over the considered electron density range. The presented results obtained for hydrated calcium sulfate ($\text{CaSO}_4 \cdot 2\text{H}_2\text{O}$) can be extended to any kind of hydrogen containing compounds.

Keywords: Stark broadening; Spectra simulation; Hydrogen; Calcium; LIBS.

1. Introduction

Stark broadening of spectral lines is under investigation since the discovery of the effect in 1913. With the diversification of the available plasma sources and the increasing interest for plasma diagnostic tools, the theoretical and experimental studies dedicated to Stark broadening became popular in the 1960's [1, 2]. Since that time, several review papers have been published to summarize the results obtained by a large number of research groups all over the world [3–7]. Despite of the numerous efforts in the past decades, precise Stark broadening parameters are still only partially available, even for the most prominent transitions. This is mainly due to the difficulties of calibrating the Stark broadening measurements using an alternative and independent measurement method. Recently, Thomson scattering was applied to measure electron density and temperature in laser-produced plasmas [8, 9]. However, the application of this method to high-density thermal plasmas

is doubtful due to electron heating by the probe laser radiation. From the theoretical point of view, there does not exist any model that enables accurate calculations of Stark broadening over a large electron density range, as illustrated by Griem for H_α [10].

The lack of accurate Stark broadening data and the need of further developments in appropriate models motivate the related research in different types of plasmas. With respect to arcs, sparks or other electrical discharges, the plasmas produced by pulsed lasers are historically younger. This is mainly due to the technological development of laser sources: reliable pulsed lasers that generate highly reproducible plasmas are available since the last two decades only. In addition, the small size and the fast expansion dynamics present particular difficulties for plasma diagnostics. With the invention of gated detectors and the development of applications such as laser-induced breakdown spectroscopy (LIBS), the investigation of plasmas produced by pulsed laser ablation stimulated a strongly growing interest in the past years. The small size and the large initial density now appear as advantages, since the former property limits the optical thickness of plasma emission, and the latter

*Corresponding author: milosb@ff.bg.ac.rs

43 feature favors the establishment of local thermal equi- 95
44 librium [11, 12]. 96

45 The expansion dynamics of plasmas produced by laser 97
46 ablation strongly depend on the irradiation conditions 98
47 and the surrounding atmosphere. The use of infrared 99
48 radiation favors the absorption of laser photons by the
49 background gas, leading to an elongated shape of the
50 plasma [13]. This condition enables rapid intermixing 100
51 of the ablated vapor with the surrounding atmosphere
52 [14]. Contrarily, the use of shorter wavelength radia- 101
53 tion increases the laser-material energy coupling. The
54 plasma screening effect [15, 16] is reduced, and the 102
55 plasma is characterized by a hemispherical shape [17]. 103
56 If, in addition to the use of the short laser wavelength, 104
57 the ablation process occurs in an argon atmosphere, the 105
58 ablation plume appears spatially almost uniform. This 106
59 was illustrated by the analysis of the spectral shapes 107
60 of resonance lines and strongly Stark-shifted transitions 108
61 [18]. 109

62 Stark broadening parameters of calcium lines are of in- 110
63 terest to laboratory plasma diagnostics, as well as for 111
64 theoretical modeling. In LIBS plasmas for example, 112
65 Ca is often present as an impurity. Also, due to its 113
66 large abundance all over the universe, calcium presents 114
67 a constituent of many stellar plasmas, and Ca and Ca⁺ 115
68 lines are of a great importance in astrophysics [19]. 116
69 The most intense lines and in particular the ionic res- 117
70 onance lines were investigated extensively in the past 118
71 [20–31]. The resonance lines are generally strongly
72 self-absorbed, and their practical usage for plasma diag- 119
73 nostics is often doubtful. Stark broadening calculations, 120
74 based on the semiclassical perturbation formalism, have
75 been performed for many Ca [19, 32] and Ca⁺ transi- 121
76 tions [33, 34]. The correlation of Stark broadening with
77 the energy gap between the upper-level of the transition
78 and the ionization potential was also investigated [35]. 122
79 However, Stark parameters of many Ca transitions in the
80 visible and UV ranges are still missing in literature. 123

81 In the present work, we take advantage of the spa- 124
82 tially uniform character of the plasma produced by UV 125
83 nanosecond laser ablation in argon at near atmospheric 126
84 pressure. Samples of hydrated calcium sulfate were ab- 127
85 lated to obtain spectral line emission from hydrogen, 128
86 calcium, oxygen and several impurities. Comparing 129
87 the measured emission spectrum to the spectral radia- 130
88 nce computed for a uniform plasma in local thermo- 131
89 dynamic equilibrium, we were able to characterize the 132
90 plasma and to deduce the Stark broadening parameters
91 for many atomic and ionic lines. With respect to the tra- 133
92 ditional methods based on space-resolved spectroscopic
93 measurements and complex data analysis via Abel in- 134
94 version [20, 28, 36], the presented method appears eas-

ier to handle and gives rapid access to a large number
of data. Indeed, using an echelle spectrometer of large
resolving power, the recording of a few spectra at dif-
ferent delays enables the determination of Stark broad-
ening parameters of a large number of spectral lines.

100 2. Method and calculation details

101 2.1. Principle of Stark broadening measurements

102 The method for the measurement of Stark broaden-
103 ing parameters consists of the following three succes-
104 sive steps: (i) the plasma temperature T , the electron
105 density n_e , and the relative fractions of elements C were
106 deduced for spectra recorded at different times (delay
107 between laser pulse and detector gate) using the itera-
108 tive procedure described in Ref. [37]. Here, n_e is de-
109 duced from H_α for which accurate electron density mea-
110 surements are expected for n_e -values of the order of
111 10^{17} cm⁻³ [10]; (ii) Once the plasma is characterized,
112 the Stark widths and shifts of non-hydrogenic lines are
113 deduced from best agreement between measured and
114 computed spectra. The plasma being characterized pre-
115 viously, the calculation of the line profiles accounts
116 for Doppler- and resonance broadening; (iii) The Stark
117 broadening parameters w and d of the non-hydrogenic
118 lines were deduced from the linear increase of Stark
119 width and shift with n_e .

120 2.2. Calculation details

121 Material ablation with pulsed lasers in a background
122 gas at near atmospheric pressure leads to almost hemi-
123 spherical expansion if the interaction of the laser beam
124 with the gas is negligible, and the laser spot diameter is
125 small compared to the plasma radius. In that case, the
126 blast wave model may be applied to describe the plume
127 expansion dynamics. The conditions are fulfilled for ul-
128 traviolet nanosecond laser pulses [13, 17]. If argon is
129 used as a buffer gas, the spatial distributions of electron
130 density and temperature within the ablated vapor are al-
131 most uniform and the spectral radiance of the plasma
132 can be calculated using [37]

$$133 I_\lambda = U_\lambda(1 - e^{-\alpha L}), \quad (1)$$

134 where U_λ is the black-body spectral radiance, L is the
135 plasma diameter along the observation direction, and α
136 is the absorption coefficient given by [1]

$$137 \alpha(\lambda) = \pi r_0 \lambda^2 f_{lu} n_l P(\lambda) (1 - e^{-hc/\lambda kT}). \quad (2)$$

138 Here, r_0 is the classical electron radius, λ is the wave-
139 length, h is the Planck constant, c is the vacuum light

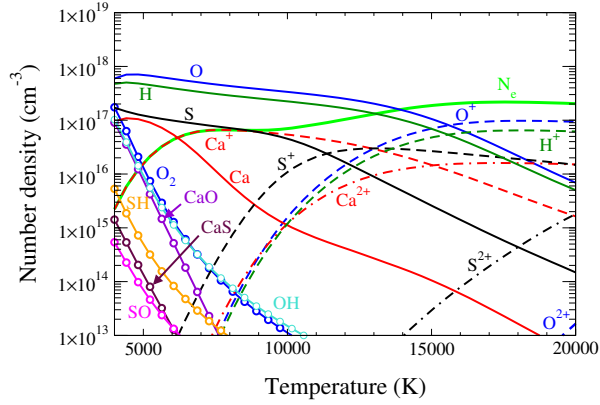


Figure 1: Number densities of species versus temperature computed for a $\text{CaSO}_4 \cdot 2\text{H}_2\text{O}$ plasma in LTE at atmospheric pressure.

velocity, k is the Boltzmann constant, f_{lu} and n_l are the absorption oscillator strength and the lower level population number density of the transition, respectively. The normalized line profile $P(\lambda)$ is calculated considering Doppler and Stark broadening that are the dominant mechanisms of spectral line broadening in strongly ionized laser-produced plasmas [38]. Depending on the relative values of Doppler and Stark widths, the line shapes are described by Gaussian, Lorentzian or Voigt profiles. The Doppler width is calculated according to plasma temperature and atomic mass of the emitting species. The Stark width is obtained using [10, 39]

$$\Delta\lambda_{\text{Stark}} = w \left(\frac{n_e}{n_e^{\text{ref}}} \right)^m, \quad (3)$$

where w is the Stark width at the reference electron density n_e^{ref} . The Stark shift is obtained from Eq. (3) replacing w by the Stark shift at the reference electron density d . We assumed linear dependence of Stark width with electron density ($m = 1$) for all non-hydrogenic lines. For the H_α transition, different m -values were reported in literature. The values obtained from theory vary from 0.68 to 0.83 whereas $m \approx 0.35$ was reported for experiments [10]. In the present work, we use for $n_e \leq 1 \times 10^{17} \text{ cm}^{-3}$ the expression proposed by Gigoso et al. [40], using Eq. (3) with $w = 1.10 \text{ nm}$, $n_e^{\text{ref}} = 1 \times 10^{17} \text{ cm}^{-3}$, and $m = 0.68$. For larger electron densities, we use a slightly different expression with a somewhat larger experimentally determined m -value (see section 4.2). We stress that Stark broadening of H_α is recognized as a reliable tool for n_e -measurements in laser-induced plasmas [41].

The lower level population number density in Eq. (2) is obtained by calculating the plasma composition assuming local thermodynamic equilibrium (LTE) [42]. The

number densities of plasma species computed for LTE are displayed in Fig. 1 for the elemental composition of the here investigated hydrated calcium sulfate sample. The calculations have been performed by setting the kinetic pressure of the plasma to atmospheric pressure [42]. As the pressure is kept constant, the atomic number densities of elements and thus the total atomic number density of the plasma decrease with increasing temperature.

In the considered temperature range, atomic and ionic species dominate the plasma composition. Molecular species significantly contribute to the plasma composition only for $T < 5,000 \text{ K}$. According to the moderate dissociation energies of the involved diatomic species [43], their number densities decrease rapidly with temperature, representing a fraction $< 1\%$ for $T = 6,000 \text{ K}$. For $T \leq 15,000 \text{ K}$, neutral atoms are the dominating plasma species according to the large ionization potentials of the most abundant elements H and O [44]. The ionization potential of Ca being of only 6 eV, the electrons originate essentially from the ionization of calcium in the temperature range up to 9,000 K. For $T > 9,000 \text{ K}$, the ionization of sulfur contributes significantly to the plasma ionization whereas $T > 12,000 \text{ K}$ is required to enable strong contributions of oxygen and hydrogen. The temperature dependence of the Ca^{2+} number density is similar to those of O^+ and H^+ . This is due to the ionization potential of Ca^+ that is close to the ionization energies of O and H. For $T > 15,000 \text{ K}$, the ionic species dominate the plasma and O^+ and H^+ ions are the most abundant species.

3. Experiment

The experiments were carried out with a frequency-quadrupled Nd:YAG laser (Quantel, model Brilliant) delivering pulses of 4 ns duration and 40 mJ energy at the wavelength of 266 nm. The laser pulse energy was attenuated to 6 mJ by turning the beam polarization with the aid of a half-wave plate and crossing through a polarization analyzer. The laser beam was focused onto the sample surface using a plano-convex lens of 150 mm focal length. According to a spot diameter of $100 \mu\text{m}$ of the Gaussian beam, a laser fluence of about 80 J cm^{-2} was obtained on the sample surface. The pellet samples were prepared from commercially available hydrated calcium sulfate powder using a hydraulic press, and placed on a motorized sample holder in a vacuum chamber of 10^{-4} Pa residual pressure. During the experiments, the chamber was filled with argon at $5 \times 10^4 \text{ Pa}$ pressure. The plasma emission was captured by imaging the plume with two lenses of 150 and 35

223 mm focal lengths onto the entrance of an optical fiber
 224 of 600 μm diameter. The optical axis of the lenses was
 225 tilted by 15° with respect to the surface normal. Accord-
 226 ing to the image magnification of about 1.5, a cylindri-
 227 cal volume of about 3 mm diameter was observed. The
 228 fiber was coupled to the entrance of an echelle spec-
 229 trometer (LTB, model Aryelle Butterfly) of 0.4 m focal
 230 length and a resolving power of 8.9×10^3 . Photon de-
 231 tection was ensured using an intensified charge-coupled
 232 device matrix detector (Andor, model IStar). The spec-
 233 tral resolution of the apparatus was measured using a
 234 low-pressure argon-mercury lamp. An intensity calibra-
 235 tion of the spectroscopic apparatus was performed in the
 236 visible and UV spectral ranges using a calibrated tung-
 237 sten lamp (Oriel, model 63358) and a deuterium lamp
 238 (Heraeus, model DO544J), respectively.
 239 The spectra were recorded for different delays of the de-
 240 tector gate t_g with respect to the laser pulse. The gate
 241 width Δt_g was adjusted for each delay so that $\Delta t_g < t_g$.
 242 We denote the measurement time $t = t_g \pm \Delta t_g/2$. To
 243 enhance the signal-to-noise ratio, data acquisition was
 244 performed by averaging over 500 ablation events, ap-
 245 plying 5 pulses to 100 different irradiation sites. The
 246 sites were separated by a distance of 150 μm .

247 4. Results and discussion

248 4.1. Plasma characterization

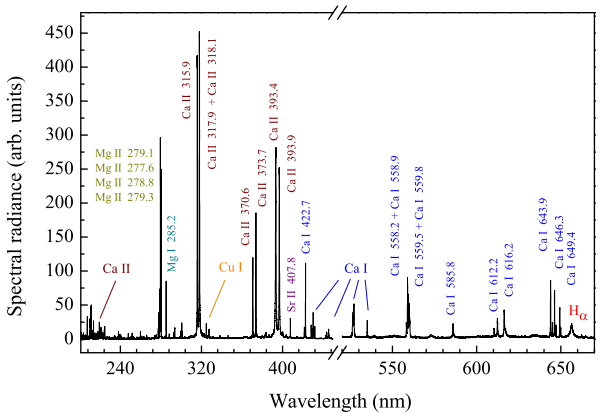


Figure 2: Spectrum recorded during ablation of hydrated calcium sulfate for $t = (475 \pm 75)$ ns.

249 The emission spectrum of the plasma produced by
 250 laser ablation of hydrated calcium sulfate is displayed
 251 in Fig. 2 for the spectral ranges that exhibit the most
 252 significant investigated transitions. To facilitate the
 253 observation of the low-intensity transitions in the green-
 254 red range, the intensity scale was multiplied by a factor

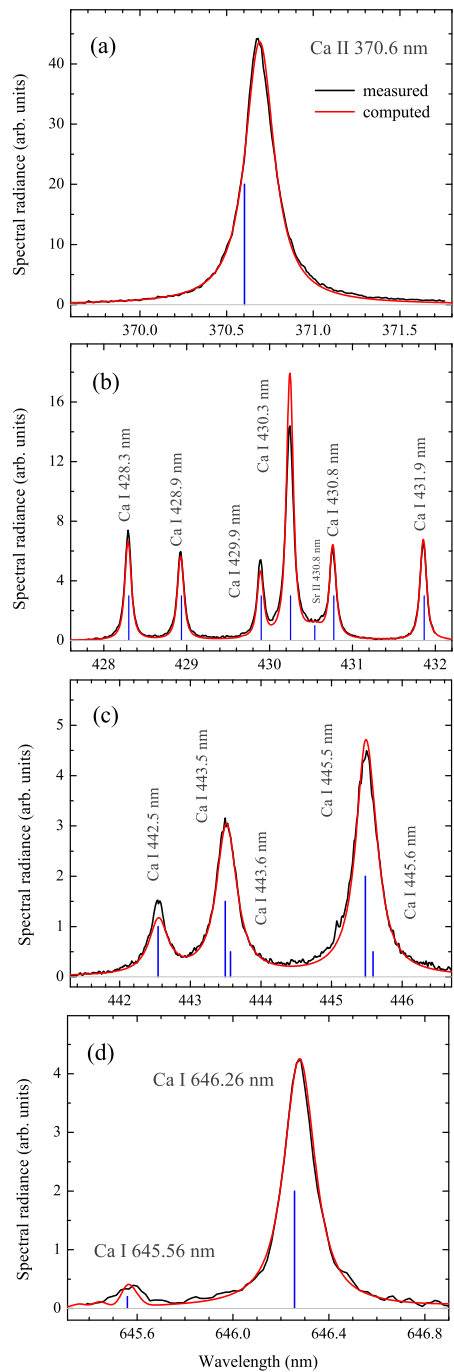


Figure 3: Measured spectrum (black line) and computed spectral radiance (red line) of various calcium transitions. The computed radiance was obtained for $T = 12,200$ K, $n_e = 1.6 \times 10^{17}$ cm^{-3} , $L = 0.65$ mm and the elemental composition given in Table 1. The blue lines denote the resonance wavelength of each transition.

of 10 for that part of the spectrum. The plasma emission is dominated by spectral lines of singly charged calcium ions. In addition, transitions of Ca neutral atoms and of species from several impurity elements are observed. We identify the strongly broadened H_α transition in the red range of the spectrum. The atomic fractions of both major and minor elements deduced from the best agreement between measured and computed spectra are given in Table 1.

The spectrum measured for $t = (475 \pm 75)$ ns (see Fig. 2) is displayed in Fig. 3 for several spectral ranges, together with the computed spectral radiance. We observe a good agreement between measured and computed spectral shapes for all presented transitions. It is shown that the lines are significantly broadened. Some transitions such as Ca II 370.6 nm (a) and Ca I 646.26 nm (d) are characterized by large Stark shifts. A slight difference in intensity is visible for some lines and in particular for Ca I 430.3 nm. The mismatch is attributed to the low accuracy of the transition probabilities [44]. The time-evolution of the laser-induced plasma was investigated by recording spectra for different observation delays with respect to the laser pulse. The characteristic behavior is illustrated in Fig. 4 where the spectral shapes of H_α (a), Ca I 585.74 nm (b), and Mg I 285.21 nm (c) are shown for different times. We observe strong broadening at early times followed by consecutive narrowing of the line profiles with increasing time. In addition, Ca I 585.74 nm and Mg I 285.21 nm exhibit large red-shifting at early times. Transitions of large Stark shift are characterized by asymmetric line shapes if they are emitted from a spatially non-uniform plasma [18]. Here, the symmetric shape observed for the Mg I 285.21 nm line (c) shows that the plasma is spatially uniform in agreement with

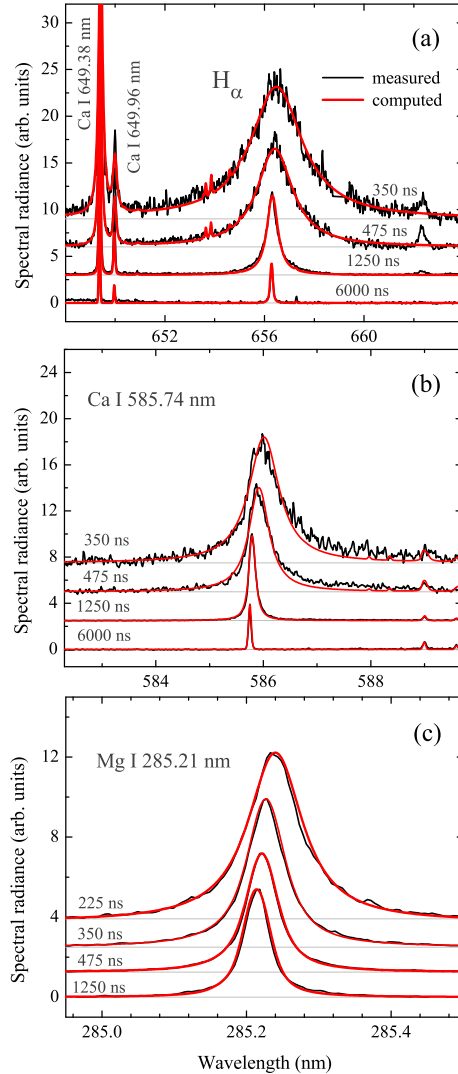


Figure 4: Measured (black line) and computed (red line) spectral radiance of several transitions for different observation times.

Table 1: Atomic fractions of the constituents of the hydrated calcium sulphate pellet deduced from the LIBS spectra C_{LIBS} . The reference values C_{ref} correspond to the chemical formula $CaSO_4 \cdot 2H_2O$.

Elmnt.	$C_{LIBS}(\%)$	$C_{ref}(\%)$
Ca	9.1	8.3
S	8.3	8.3
O	47	50.0
H	35	33.3
Cu	0.04	-
Fe	0.014	-
Li	0.017	-
Mg	0.4	-
Si	0.08	-
Sr	0.012	-

previous observations of LIBS plasmas produced in argon background gas [37, 45].

The plasma temperature evolution is illustrated by the Saha-Boltzmann plots displayed in Fig. 5. Here, ϵ is the emission coefficient deduced from the measurements using $\epsilon = \epsilon_c I_m / I_c$, where ϵ_c is the calculated emission coefficient, and I_m and I_c are the measured and computed line-integrated spectral radiances, respectively. As the computed radiance intrinsically accounts for self-absorption, the Saha-Boltzmann plot displayed in Fig. 5 is equivalent to the Boltzmann plot corrected for self-absorption presented by Bulajic et al. [46]. It is

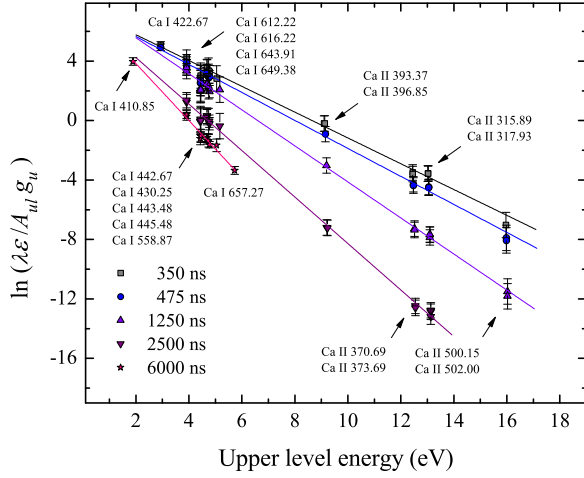


Figure 5: Saha-Boltzmann plots of calcium for various observation times.

shown that the population number densities of atomic and ionic excited species are well described by the equilibrium distribution for all measurement times.

The deduced values of temperature and electron density are shown in Fig. 6 as functions of time. The horizontal error bars represent the gate width, whereas the vertical error bars stand for the measurement uncertainties. According to Griem [10], electron density measurements using H_α are most precise for n_e -values close to 10^{17} cm^{-3} . The measurement error increases with distance from that value due to the uncertainty of the exponent m (see Eq. 3). We estimated the n_e -measurement error assuming uncertainties of 10% for the parameters w and m and of 5% for the Stark width measurement. During the considered time-interval from 200 to 6000 ns, the electron density decreases by more than two orders of magnitude from 5×10^{17} to $3 \times 10^{15} \text{ cm}^{-3}$, whereas the temperature diminishes from about 14,000 to 6,000 K.

4.2. Stark width and shift measurements

The strong variation of electron density over the measured time-interval and the spatially uniform character of the laser-produced plasma are now explored to measure the Stark widths and shifts of spectral lines. We emphasize that the calculation of the spectral radiance allows us to predict the optical thickness of each transition, and thus to exclude strongly self-absorbed lines from the analysis. For some transitions such as resonance lines of neutral atoms, the optical thickness critically depends on the observation delay. At early time, when the plasma temperature is high and ionic species

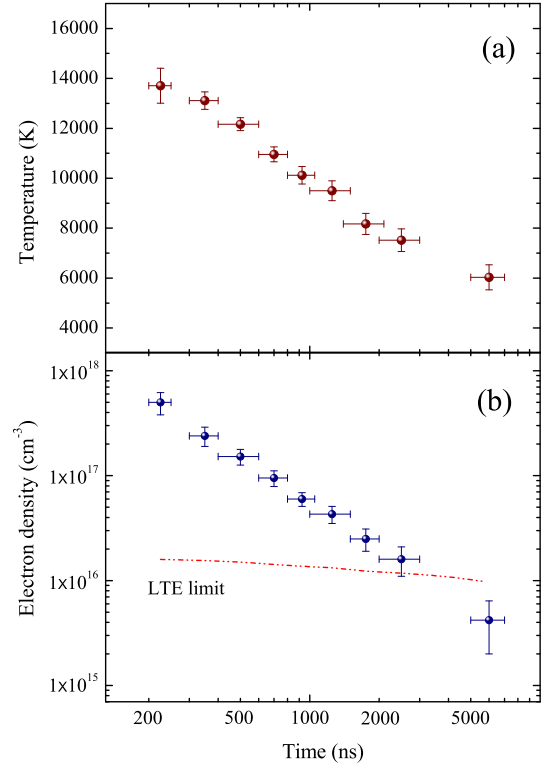


Figure 6: Temporal evolution of electron density (a) and excitation temperature (b). The dashed red line (b) stands for the minimum n_e -value required for LTE according to the McWhirter criterion [47].

dominate (see Fig. 1), the ground state population number densities of neutral atoms are small and their resonance lines have little optical thickness. Contrarily, at late times, when the temperature is low, neutral atoms dominate, their ground state population number densities are large, and self-absorption of resonance lines is strong.

For transitions of large Stark shift, the influence of the optical thickness on the spectral line shape can be verified by analyzing the correlation between Stark width and shift. This is illustrated in Fig. 7, where the linear increase of Stark shift with Stark width is observed for transitions of Ca and Ca^+ .

The spectral lines having small optical thickness over the entire time-interval were used to analyse the dependence of their Stark widths and shifts on the Stark width of the H_α transition. This is shown in Fig. 8 where the Stark width of Ca I 585.74 nm is presented versus H_α Stark width on a logarithmic scale. Assuming linear dependencies of Stark width with electron density for non-hydrogenic transitions, we can deduce from the slope the exponent m that characterizes the dependence of the H_α Stark width on n_e (see Eq. 3). We observe in

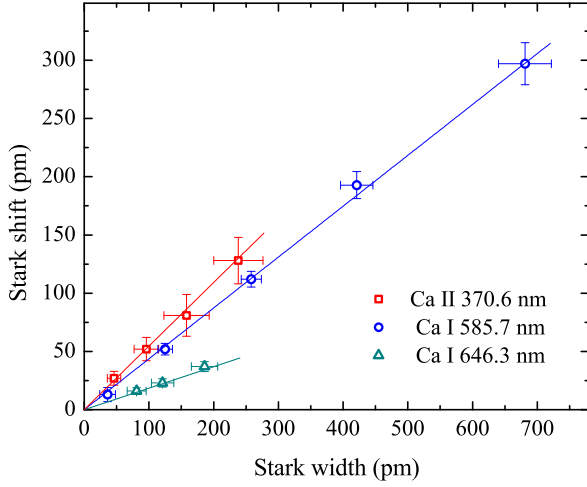


Figure 7: Stark shift vs Stark width of calcium lines deduced from measurements at various delays.

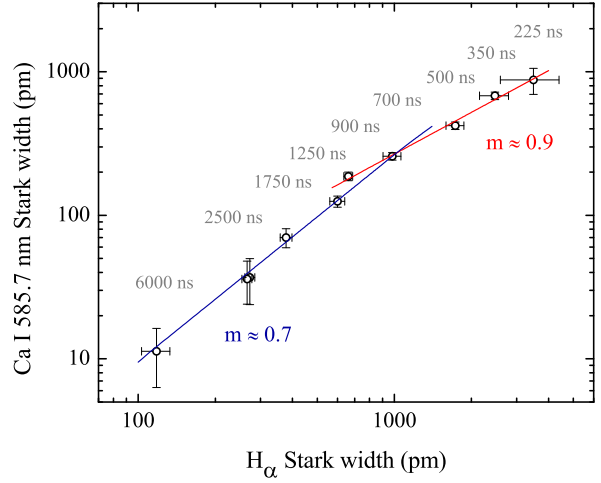


Figure 8: Stark width of a non-hydrogenic transition vs H_α Stark width. We deduce slightly different m -values for H_α Stark broadening (see Eq. 3) for the n_e -ranges below and above $1 \times 10^{17} \text{ cm}^{-3}$.

357 Fig. 8 two slightly different slopes, indicating that the
 358 n_e -dependence of H_α Stark broadening in the low elec-
 359 tron density range differs from that at large n_e -values.
 360 The transition between both regimes corresponds to a
 361 delay ≈ 1000 ns for which the electron density is close
 362 to $1 \times 10^{17} \text{ cm}^{-3}$. We thus describe Stark broadening
 363 of H_α using Eq. (3) with $w = 1.10$ nm according to liter-
 364 ature [40, 48] and $m = 0.7$ or $m = 0.9$ for electron
 365 densities below or above $n_e^{ref} = 1 \times 10^{17} \text{ cm}^{-3}$, respec-
 366 tively. It is noted that the expression equals that pro-
 367 posed by Gigosos et al. [40] and Konjevic et al. [48]
 368 for $n_e < 1 \times 10^{17} \text{ cm}^{-3}$ whereas it differs at larger elec-
 369 tron densities by the m -value exclusively. According to
 370 the good agreement between measured and computed
 371 Stark widths for $n_e \approx 1 \times 10^{17} \text{ cm}^{-3}$ reported in litera-
 372 ture [10] (see section 2) we estimate the uncertainty to
 373 $\approx 10\%$ for n_e -values close to n_e^{ref} . The error increases
 374 with distance from the reference electron density due to
 375 the uncertainty of m .
 376

377 4.3. Determination of Stark broadening parameters

378 After the implementation of the electron density
 379 measurement procedure using H_α , we explore now
 380 the linear dependence of Stark widths and shifts on
 381 n_e for non-hydrogenic transitions to determine their
 382 Stark broadening parameters w and d . Therefore, the
 383 Stark widths and shifts of non-hydrogenic transitions
 384 were measured for the spectra recorded with different
 385 delays and plotted as functions of electron density
 386 as shown in Fig. 9. According to the precise linear
 387 increase, the relative errors arising from the linear

388 analysis are small compared to the absolute errors
 389 associated to the electron density measurement using
 390 H_α . Thus, for isolated lines of measurable Stark width
 391 over a large n_e -range, the errors of the deduced w - and
 392 d -values are close to those of the most accurate n_e -
 393 measurements, evaluated to about 15%. For transitions
 394 having measurable Stark width in a restricted n_e -range
 395 only, the measurement errors of w and d are naturally
 396 larger.
 397

398 The deduced broadening parameters are presented in
 399 Tables 2 and 3 for the spectral lines of calcium and other
 400 elements, respectively. Assuming an accuracy of elec-
 401 tron density measurements of about 15% for n_e -values
 402 close to 10^{17} cm^{-3} , the estimated w -measurement error
 403 ranges from 20 to 30% for most transitions. For some
 404 lines, the accuracy is lower due to larger contributions
 405 of apparatus- and/or resonance broadening to the line
 406 profile. Compared to Stark broadening parameters re-
 407 ported in literature (see last two columns in the Tables),
 408 a mismatch larger than the estimated accuracy is ob-
 409 served for several lines. Depending on the multiplet,
 410 the values reported in literature are larger or smaller
 411 than the broadening parameters we report here. The
 412 large dispersion w - and d -values measured in different
 413 experiments is attributed to two main causes: (i) the
 414 uncertainty of electron density due to the difficulties of
 415 calibrating the n_e -measurements. Indeed, absolute val-
 416 ues of electron density are exclusively obtained through
 417 the calculation of Stark broadening parameters leading
 418 to a large variability of n_e that depends on the chosen

Table 2: Wavelength λ , configuration and term of upper and lower excitation levels of transitions according to NIST [44]. The measured Stark width w and shift d and the values reported in literature w^{lit} and d^{lit} are given for $n_e = 1 \times 10^{17} \text{ cm}^{-3}$. $\Delta w/w$ and $\Delta d/d$ are the relative errors of the measured Stark width and shift, respectively.

Species	λ (nm)	Lower level Config.	Term	Upper level Config.	Term	w (pm)	$\Delta w/w$ (%)	d (pm)	$\Delta d/d$ (%)	w^{lit} (pm)	d^{lit} (pm)
Ca I	299.496 299.732 300.086 300.686 300.921	$3p^6 4s 4p$	$^3P^o$	$3p^6 3d^2$	3P	23	20	4.4	30	29 ^a	-
Ca I	422.673	$3p^6 4s^2$	1S	$3p^6 4s 4p$	$^1P^o$	32	60	6	40	-	-
Ca I	429.899 430.253 430.774 431.865	$3p^6 4s 4p$	$^3P^o$	$3p^6 4p^2$	3P	40	25	-8	40	-	-
Ca I	442.544 443.496 443.568 445.478 445.589 445.662	$3p^6 4s 4p$	$^3P^o$	$3p^6 4s 4d$	3D	200	20	-	-	15.5 ^a	-
Ca I	558.197 558.875 559.011 559.446 559.848	$3p^6 3d 4s$	3D	$3p^6 3d 4p$	$^3D^o$	90	20	28	30	-	-
Ca I	585.745	$3p^6 4s 4p$	$^1P^o$	$3p^6 4p^2$	1D	260	20	100	20	-	-
Ca I	612.222	$3p^6 4s 4p$	$^3P^o$	$3p^6 4s 5s$	3S	165	20	75	20	-	-
Ca I	643.908 646.257 649.378	$3p^6 3d 4s$	3D	$3p^6 3d 4p$	$^3F^o$	66	20	14	30	-	-
Ca II	210.324 211.276	$3p^6 4p$	$^2P^o$	$3p^6 5d$	2D	104	20	30	20	67 ^b 73 ^b	23 ^b 26 ^b
Ca II	370.602 373.690	$3p^6 4p$	$^2P^o$	$3p^6 5s$	2S	79	25	47	20	135 ^d 183 ^d	35 ^c 35 ^c

^a Ref. [25], ^b Ref. [31], ^c Ref. [28], ^d Ref. [24].

Table 3: Wavelength λ , configuration and term of upper and lower excitation levels of transitions according to NIST [44]. The measured Stark width w and shift d and the values reported in literature w^{lit} and d^{lit} are given for $n_e = 1 \times 10^{17} \text{ cm}^{-3}$. $\Delta w/w$ and $\Delta d/d$ are the relative errors of the measured Stark width and shift, respectively.

Species	λ (nm)	Lower level Config.	Term	Upper level Config.	Term	w (pm)	$\Delta w/w$ (%)	d (pm)	$\Delta d/d$ (%)	w^{lit} (pm)	d^{lit} (pm)
C I	247.856	$2s^2 2p^2$	1S	$3s^2 2p 3s$	$^3P^o$	14	30	8	25	6.8^e	2.6^e
Cu II	212.604	$3d^9(^2D)4s$	3D	$3d^9(^2D)4p$	$^3F^o$	6	30	1.1	50	8.2^f	-
Mg I	213.598										
Mg I	277.669	$3s 3p$	$^3P^o$	$3p^2$	3P	7	40	1	100	-	-
	277.827										
	278.141										
	278.297										
Mg I	285.212	$2p^6 3s^2$	1S	$3s 3p$	$^1P^o$	17	30	8.5	30	-	-
Mg I	382.935	$3s 3p$	$^3P^o$	$3s 3d$	3D	270	20	-45	30	110^g	-2^g
	383.230										
	383.829										
Mg I	516.732	$3s 3p$	$^1P^o$	$3s 4s$	3S	90	20	50	20	33^g	9^g
	517.268									35.5^g	8.4^g
	518.360									35^g	7.4^g
Mg II	279.077	$2p^6 3p$	$^2P^o$	$2p^6 3d$	2D	30	20	9	25	162^h	22^h
	279.799									144^h	19^h
Mg II	292.863	$2p^6 3p$	$^2P^o$	$2p^6 4s$	2S	50	20	23	20	29^i	57^i
	293.651									30^i	68^i
Si I	250.689	$3s^2 3p^2$	3P	$3s^2 3p 4s$	$^3P^o$	14	25	8	25	14.1^j	-
	251.431									11.2^j	
	251.611									11.7^j	
	251.920									11.2^j	
	252.410									10.4^j	
	252.850									10.7^j	
Fe II	238.203	$3d^6(^5D)4s$	a^6D	$3d^6(^5D)4p$	z^6F^o	5	30	2	30	-	-
	238.862										
	239.562										
	239.924										
	240.488										
	241.051										
Fe II	259.587	$3d^6(^5D)4s$	a^6D	$3d^6(^5D)4p$	z^6D^o	6	30	0.8	60	-	-
	259.836										
	259.939									4.5^k	-
	260.708										
	261.187										
	261.382										
Fe II	273.954	$3d^6(^5D)4s$	a^4D	$3d^6(^5D)4p$	z^4D^o	9	30	3	35	5.3^l	-
O I	777.194	$2s^2 2p^3(^4S^o)3s$	$^5S^o$	$2s^2 2p^3(^4S^o)3p$	5P	105	35	15	40	-	-
	777.416										
	777.538										
Sr II	407.770	$4p^6 5s$	2S	$4p^6 5p$	$^2P^o$	41	20	-3.4	30	-	-
	421.551										

^e Ref. [49], ^f Ref. [50], ^g Ref. [51], ^h Ref. [52], ⁱ Ref. [53], ^j Ref. [54], ^k Ref. [55], ^l Ref. [56].

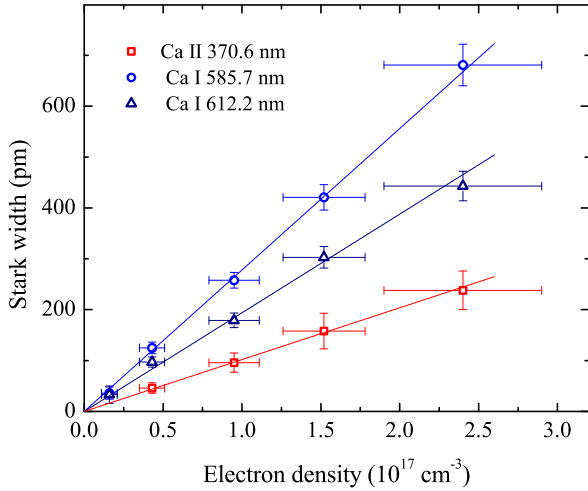


Figure 9: Stark widths of Ca I and Ca II transitions vs electron density.

419 transition and the n_e -range. (ii) The measurements re-
 420 ported in literature were performed using various types
 421 of plasmas characterized by different temperatures. Al-
 422 though the T -dependence was neglected in the present
 423 work according to the moderate temperature variation in
 424 the laser-produced plasma, the changes of Stark broad-
 425 ening parameters with temperature cannot be neglected
 426 in case of strong T -variation.
 427 As an example, the large variability of Stark broadening
 428 parameters in literature is illustrated by the w -values of
 429 6.8 and 54 pm reported for C I 247.85 nm [3, 49]. We
 430 stress that the most intense spectral lines (see Fig. 2)
 431 were not considered as their large optical thickness pre-
 432 vent the accurate Stark width measurement.

433 5. Conclusion

434 We presented a method for the measurement of Stark
 435 broadening parameters based on modeling of the emis-
 436 sion spectrum from a laser-induced plasma. Produc-
 437 ing ablation with ultraviolet nanosecond laser pulses in
 438 argon at near atmospheric pressure, the measurements
 439 take advantage of the spatially uniform distributions of
 440 electron density and temperature within the ablated va-
 441 por plume. These properties enable simple and accurate
 442 modeling based on the calculation of the spectral radi-
 443 ance of a plasma in local thermodynamic equilibrium.
 444 The spectra recording with an echelle spectrometer of
 445 large resolving power give access to analysis of a large
 446 number of spectral lines. Using hydrated calcium sul-
 447 phate as sample material, we were able to deduce the
 448 Stark broadening parameters of atomic and ionic spec-
 449 tral lines from calcium, oxygen and several impurity el-

450 ements by their simultaneous observation with the H_α
 451 transition. By varying the delay of the detector gate with
 452 respect to the laser pulse, the electron density was varied
 453 by more than two orders of magnitude from 3×10^{15}
 454 to $5 \times 10^{17} \text{ cm}^{-3}$ whereas temperature was changed
 455 from about 6,000 to 14,000 K. Assuming a linear in-
 456 crease of Stark widths of non-hydrogenic lines with n_e ,
 457 the present analysis indicate a change of the H_α Stark
 458 width-dependence on n_e that occurs when the electron
 459 density varies from values $< 10^{17} \text{ cm}^{-3}$ to larger density.
 460 For $n_e > 10^{17} \text{ cm}^{-3}$, we observe a more *non-hydrogenic*
 461 behaviour whereas the typical $n_e^{2/3}$ -dependence was re-
 462 trieved for the low electron density range, in agreement
 463 with theoretical predictions. According to the precise
 464 electron density measurements for n_e -values close to
 465 $1 \times 10^{17} \text{ cm}^{-3}$, the deduced Stark broadening param-
 466 eters have fair uncertainties of 20 to 30% for most of the
 467 investigated transitions.

468 6. Acknowledgements

The authors acknowledge the financial support
 469 provided by LASERLAB- EUROPE (grant agreement
 470 No. 284464, project CNRS-LP3002148). This research
 471 has also been supported by the Ministry of education,
 472 science and technological development of the Republic
 473 of Serbia (project ON171008).

- 476 [1] H. R. Griem, Plasma spectroscopy, Academic Press, New York,
 477 1964.
- 478 [2] H. R. Griem, Spectral line broadening of plasmas, Academic
 479 Press, New York, 1974.
- 480 [3] N. Konjević, J. R. Roberts, A critical review of the Stark widths
 481 and shifts of spectral lines from non-hydrogenic atoms, J. Phys.
 482 Chem. Ref. Data 5 (1976) 209–257.
- 483 [4] N. Konjević, M. S. Dimitrijević, W. L. Wiese, Experimental
 484 Stark widths and shifts for spectral lines of neutral atoms (A
 485 critical review of selected data for the period 1976 to 1982), J.
 486 Phys. Chem. Ref. Data 13 (1984) 619–647.
- 487 [5] N. Konjević, A. Lesage, J. R. Führ, W. L. Wiese, Experimental
 488 Stark widths and shifts for spectral lines of neutral and ionized
 489 atoms (A critical review of selected data for the period 1983
 490 through 1988), J. Phys. Chem. Ref. Data 19 (1990) 1307–1385.
- 491 [6] N. Konjević, A. Lesage, J. R. Führ, W. L. Wiese, Experimental
 492 Stark widths and shifts for spectral lines of neutral and ionized
 493 atoms (A critical review of selected data for the period 1989
 494 through 2000), J. Phys. Chem. Ref. Data 31 (2002) 819–921.
- 495 [7] A. Lesage, Experimental Stark widths and shifts for spectral
 496 lines of neutral and ionized atoms A critical review of selected
 497 data for the period 2001–2007, N. Astron. Rev. 52 (2009) 471–
 498 535.
- 499 [8] A. Mendys, K. Dzierżęga, M. Grabciec, S. Pellerin, B. P. G., Tra-
 500 vaillé, B. Bousquet, Investigations of laser-induced plasma in
 501 argon by thomson scattering, Spectrochim. Acta Part B: Atom.
 502 Spectrosc. 66 (2011) 691–697.
- 503 [9] M. Cvejić, K. Dzierżęga, T. Pięta, Investigation of thermody-
 504 namic equilibrium in laser-induced aluminum plasma using the

- 505 H_{α} line profiles and Thomson scattering spectra, *Appl. Phys. Lett.* 107 (2015) 024102 1–4.
- 506 [10] H. Griem, Stark broadening of the hydrogen Balmer- α line in
507 low and high density plasmas, *Contrib. Plasma Phys.* 40 (2000)
508 46–56.
- 509 [11] S. Eliezer, A. D. Krumbein, D. Salzmann, Generalized valid-
510 ity condition for local thermodynamic-equilibrium in a laser-
511 produced plasma, *J. Phys. D: Appl. Phys.* 11 (1978) 1693–1701.
- 512 [12] G. Cristoforetti, E. Tognoni, L. A. Gizzi, Thermodynamic equi-
513 librium states in laser-induced plasmas: From the general case to
514 laser-induced breakdown spectroscopy plasmas, *Spectrochim.*
515 *Acta Part B: Atom. Spectrosc.* 90 (2013) 1–22.
- 516 [13] M. Boueri, M. Baudelet, J. Yu, X. Mao, S. S. Mao, R. Russo,
517 Early stage expansion and time-resolved spectral emission of
518 laser-induced plasma from polymer, *Appl. Surf. Sci.* 255 (2009)
519 9566–9571.
- 520 [14] Q. Ma, V. Motto-Ros, F. Laye, J. Yu, W. Lei, X. Bai, L. Zheng,
521 H. Zeng, Ultraviolet versus infrared: Effects of ablation laser
522 wavelength on the expansion of laser-induced plasma into one-
523 atmosphere argon gas, *J. Appl. Phys.* 111 (2012) 1–11.
- 524 [15] I. N. Mihailescu, J. Hermann, Laser-plasma interactions, in:
525 P. Schaaf (Ed.), *Laser Processing of Materials*, Springer, Berlin,
526 2010, pp. 49–88.
- 527 [16] M. Burger, D. Pantić, Z. Nikolić, S. Djeniže, Shielding effects
528 in the laser-generated copper plasma under reduced pressures of
529 He atmosphere, *J. Quant. Spectrosc. Radiat. Transf.* 170 (2016)
530 19–27.
- 531 [17] L. Mercadier, J. Hermann, C. Grisolia, A. Semerok, Diagnostics
532 of nonuniform plasmas for elemental analysis via laser-induced
533 breakdown spectroscopy: demonstration on carbon-based materi-
534 als, *J. Anal. At. Spectrom.* 28 (2013) 1446–1455.
- 535 [18] J. Hermann, C. Gerhard, E. Axente, C. Dutouquet, Comparative
536 investigation of laser ablation plumes in air and argon by anal-
537 ysis of spectral line shapes: Insights on calibration-free laser-
538 induced breakdown spectroscopy, *Spectrochim. Acta Part B:*
539 *Atom. Spectrosc.* 100 (2014) 189–196.
- 540 [19] M. S. Dimitrijević, S. Sahal-Bréchet, Stark broadening of neu-
541 tral calcium spectral lines, *Astron. Astrophys. Supp.* 140 (1999)
542 191–192.
- 543 [20] J. Chapelle, S. Sahal-Bréchet, Experimental and theoretical
544 electron impact broadening of some Mg II and Ca II lines of
545 astrophysical interest, *Astron. Astrophys.* 6 (1970) 415–422.
- 546 [21] J. S. Hildum, J. Cooper, Stark broadening of calcium ion res-
547 onance lines, *Phys. Lett.* 36A (1971) 153–155.
- 548 [22] J. Purić, N. Konjević, Stark shifts of some isolated spectral lines
549 of singly ionized earth alkaline metals, *Z. Phys.* 249 (1972) 440–
550 444.
- 551 [23] W. W. Jones, A. Sanchez, J. R. Greig, H. R. Griem, Measure-
552 ment and calculation of the Stark-broadening parameters for the
553 resonance lines of singly ionized calcium and magnesium, *Phys.*
554 *Rev. A* 5 (1972) 2318–2328.
- 555 [24] H. Kusch, H. Pritschow, Broadening and shift of calcium lines
556 by microfields, *Astron. Astrophys.* 4 (1970) 31–35.
- 557 [25] R. Hühn, H. Kusch, Broadening and shift of calcium lines by
558 van der Waals interaction with argon atoms and by electron im-
559 pact, *Astron. Astrophys.* 28 (1973) 159–164.
- 560 [26] D. Hadžiomerspahić, M. Platiša, N. Konjević, M. Popović, Stark
561 broadening and shift of some isolated spectral lines of singly
562 ionised earth alkaline metals, *Z. Phys.* 262 (1973) 169–179.
- 563 [27] J. F. Baur, J. Cooper, A shock tube study of line broadening
564 in a temperature range of 6100 to 8300 K, *J. Quant. Spectrosc.*
565 *Radiat. Transf.* 17 (1977) 311–322.
- 566 [28] C. Fleurier, S. Sahal-Bréchet, J. Chapelle, Stark profiles of some
567 ion lines of alkaline earth elements, *J. Quant. Spectrosc. Radiat.*
568 *Transf.* 17 (1977) 595–604.
- 569 [29] C. Goldbach, G. Nollez, P. Plomdeur, J.-P. Zimmermann, Stark-
570 width measurements of singly ionized calcium resonance lines
571 in a wall-stabilized arc, *Phys. Rev. A* 28 (1983) 234–237.
- 572 [30] A. Srečković, S. Djeniže, Measured Stark width and shift of
573 393.367 nm Ca II resonance spectral line, *Bull. Astron. Belgr.*
574 148 (1993) 7–10.
- 575 [31] J. A. Aguilera, C. Aragón, J. Manrique, Measurement of Stark
576 widths and shifts of Ca II spectral lines, *MNRAS* 444 (2014)
577 1854–1858.
- 578 [32] M. S. Dimitrijević, S. Sahal-Bréchet, Stark broadening param-
579 eter tables for neutral calcium spectral lines, *Serb. Astron. J.* 161
580 (2000) 39–88.
- 581 [33] M. S. Dimitrijević, S. Sahal-Bréchet, Stark broadening param-
582 eter tables for Ca II lines of astrophysical interest, *Bull. Astron.*
583 *Belgr.* 145 (1992) 81–99.
- 584 [34] M. S. Dimitrijević, S. Sahal-Bréchet, Stark broadening of Ca
585 II spectral lines, *J. Quant. Spectrosc. Radiat. Transf.* 49 (1993)
586 157–164.
- 587 [35] I. Tapalaga, I. P. Dojčinović, M. K. Milosavljević, J. Purić, Stark
588 width regularities within neutral calcium spectral series, *Publ.*
589 *Astron. Soc. Aust.* 29 (2012) 20–28.
- 590 [36] M. Cirisan, M. Cvejić, M. Gavrilović, S. Jovicević, N. Konjević,
591 J. Hermann, Stark broadening measurement of Al II lines in a
592 laser-induced plasma, *J. Quant. Spectrosc. Radiat. Transf.* 133
593 (2014) 652–662.
- 594 [37] C. Gerhard, J. Hermann, L. Mercadier, L. Loewenthal, E. Ax-
595 ente, C. Luculescu, T. Sarnet, M. Sentis, W. Viöl, Quantitative
596 analyses of glass via laser-induced breakdown spectroscopy in
597 argon, *Spectrochim. Acta Part B: Atom. Spectrosc.* 101 (2014)
598 32–45.
- 599 [38] X. Z. Zhao, L. J. Shen, T. X. Lu, K. Niemax, Spatial distri-
600 butions of electron-density in microplasmas produced by laser
601 ablation of solids, *Appl. Phys. B: Photophys. Laser Chem.* 55
602 (1992) 327–330.
- 603 [39] E. Tognoni, V. Palleschi, M. Corsi, G. Cristoforetti,
604 N. Omenetto, I. Gornushkin, B. W. Smith, J. D. Winefordner,
605 From sample to signal in laser-induced breakdown spectro-
606 scopy: a complex route to quantitative analysis, in: A. W.
607 Miziolek, V. Palleschi, I. Schechter (Eds.), *Laser-induced break-*
608 *down spectroscopy*, Cambridge University, Berlin, 2006, pp.
609 122–194.
- 610 [40] M. A. Gigosos, M. A. Gonzalez, V. Cardenoso, Computer sim-
611 ulated Balmer-alpha, -beta, and -gamma Stark line profiles for
612 non-equilibrium plasma diagnostics, *Spectrochim. Acta Part B:*
613 *Atom. Spectrosc.* 58 (2003) 1489–1504.
- 614 [41] A. D. Giacomo, M. Dell’Aglio, R. Gaudiuso, G. Cristoforetti,
615 S. Legnaioli, V. Palleschi, E. Tognoni, Spatial distribution of
616 hydrogen and other emitters in aluminum laser-induced plasma
617 in air and consequences on spatially integrated laser-induced
618 breakdown spectroscopy measurements, *Spectrochim. Acta Part*
619 *B: Atom. Spectrosc.* 63 (9) (2008) 980–987.
- 620 [42] J. Hermann, A. Lorusso, A. Perrone, F. Strafella, C. Dutouquet,
621 B. Torralba, Simulation of emission spectra from nonuniform
622 reactive laser-induced plasmas, *Phys. Rev. E* 92 (2015) 1–15.
- 623 [43] A. Radzig, B. Smirnov, Reference Data on Atoms, Molecules
624 and Ions, Springer, Berlin, 1985.
- 625 [44] A. Kramida, Y. Ralchenko, J. Reader, Nist Atomic Spectra
626 Database, National Institute of Standards and Technology,
627 Gaithersburg, MD (2016).
628 URL <http://physics.nist.gov/asd>
- 629 [45] M. Burger, M. Skočić, M. Ljubisavljević, Z. Nikolić, S. Djeniže,
630 Spectroscopic study of the laser-induced indium plasma, *Eur.*
631 *Phys. J. D* 68 (2014) 223:1–8.
- 632 [46] D. Bulajic, M. Corsi, G. Cristoforetti, S. Legnaioli, V. Palleschi,
633 A. Salvetti, E. Tognoni, A procedure for correcting self-
634

- 635 absorption in calibration free-laser induced breakdown spec-
636 troscopy, *Spectrochim. Acta Part B: Atom. Spectrosc.* 57 (2002)
637 339–353.
- 638 [47] R. McWhirter, Ch. 5, in: R. H. Huddlestone (Ed.), *Plasma Diag-*
639 *nostic Techniques*, Academic, New York, 1965, pp. 201 – 264.
- 640 [48] N. Konjević, M. Ivković, N. Sakan, Hydrogen Balmer lines for
641 low electron density plasma diagnostics, *Spectrochim. Acta Part*
642 *B: Atom. Spectrosc.* 76 (2012) 16–26.
- 643 [49] S. Djeniže, A. Srečković, S. Bukvić, The C I 247.8561 nm reso-
644 nance line stark broadening parameters, *Z. Naturfors. Sect. A-J.*
645 *Phys. Sci.* 61 (2006) 91–94.
- 646 [50] M. Skočić, M. Burger, Z. Nikolić, S. Bukvić, S. Djeniže, Stark
647 broadening in the laser-induced Cu I and Cu II spectra, *J. Phys.*
648 *B* 46 (2013) 185701:1–6.
- 649 [51] S. Djeniže, S. Bukvić, A. Srečković, Stark broadening and tran-
650 sition probability ratios in the Mg I spectrum, *Astron. Astro-*
651 *phys.* 425 (2004) 361–365.
- 652 [52] S. Bukvić, A. Srečković, S. Djeniže, Mg II h and k lines Stark
653 parameters, *New Astron.* 9 (2004) 629–633.
- 654 [53] S. Djeniže, S. Bukvić, A. Srečković, M. Platiša, Mg II spectral
655 line broadening in helium, oxygen and argon-helium plasmas,
656 *Astron. Astrophys.* 424 (2004) 561–564.
- 657 [54] S. Bukvić, S. Djeniže, A. Srečković, Line broadening in the Si
658 I, Si II, Si III, and Si IV spectra in the helium plasma, *Astron.*
659 *Astrophys.* 508 (2009) 491–500.
- 660 [55] C. Aragón, J. Aguilera, J. Manrique, Measurement of Stark
661 broadening parameters of Fe II and Ni II spectral lines by laser
662 induced breakdown spectroscopy using fused glass samples, *J.*
663 *Quant. Spectrosc. Radiat. Transf.* 134 (2014) 39–45.
- 664 [56] C. Aragón, P. Vega, J. Aguilera, Stark width measurements of
665 Fe II lines with wavelengths in the range 260-300 nm, *J. Phys.*
666 *B* 44 (2011) 55002:1–7.